Mechanistic Investigation of Bisphenol A Removal by Gel-Floc Structures Synergistically Formed from Crayfish Shell Biochar and Sodium Alginate

Haowen Feng[a], Sisi Que[a*], Liang Wang[b*], Jiaqin Zeng[a]

[a] School of River and Ocean Engineering, Chongqing Jiaotong University, Chongqing 400074, China

[b] School of Resources and Safety Engineering, Chongqing University, Chongqing, China

*to whom all correspondence should be addressed:

sisique@126.com, lw38c@cqu.edu.cn

Graphical abstract

Abstract

Bisphenol A (BPA), a representative endocrine-disrupting chemical, is widely present in aquatic environments and poses potential risks to ecosystems and human health. In conventional water treatment, the presence of natural organic matter (NOM), particularly polysaccharides, often interferes with pollutant removal and reduces treatment efficiency. In this study, a Ca-rich biochar (BCFS800) was prepared from restaurant-derived crayfish shell waste to investigate the

mechanism of synergistic BPA removal with a natural polysaccharide, sodium alginate (SA). The results show that hydroxyl-calcium species enriched on the BCFS800 surface can crosslink with SA to form stable gel-like flocs, thereby enhancing BPA removal. Under the conditions of BCFS800 2.5 g/L, SA 50 mg/L, initial pH 6, rapid mixing at 250 r/min for 10 min, and slow mixing at 60 r/min for 10 min, BPA removal reached approximately 76%, and effluent turbidity decreased markedly, indicating favorable treatment performance and settling behavior. Characterizations by BET, SEM, XRD, FTIR, and XPS demonstrate that ball milling increased the specific surface area and promoted the exposure of Ca-based reactive sites, strengthening the crosslinking capability between BCFS800 and SA and improving floc formation. Mechanistic analysis suggests that BPA removal by the gel-like flocs is mainly driven by sweep flocculation coupled with surface adsorption, accompanied by π–π interactions and hydrogen bonding. Overall, this work demonstrates that Ca-rich crayfish shell biochar can convert natural polysaccharides from adsorption interferents into building units for gel-floc construction, providing new insights and support for green water treatment under NOM-impacted conditions.

Keywords: crayfish shell biochar; bisphenol A; natural polysaccharides; sodium alginate; flocculation; biochar flocs; adsorption.

1.Introduction

Bisphenol A (BPA) is an organic chemical widely used in the manufacture of polycarbonates and epoxy resins, while also being a representative environmental endocrine-disrupting chemical (EDC) (Werkneh et al., 2022). Owing to its estrogen-like molecular structure and high biological activity, BPA is frequently detected in surface water, groundwater, and municipal wastewater (Abu Hasan et al., 2023). BPA is a highly mobile substance that is persistent in the environment and thus has become a globally important water pollutant of interest (Liu et al., 2016). The most recent methods in the area of BPA extraction entail primarily membrane separation (Noor et al., 2022), photocatalysis (Huang et al., 2024), adsorption (Sujatha et al., 2025) as well as coagulation (Tian et al., 2019). Nevertheless, ubiquitous natural organic matter (natural organic matter, NOM) may be a part of and disrupt these treatment processes (Yu et al., 2023). In particular, NOM can grow an organic fouling film on surfaces of membranes, causing a decrease in flux and irreversible fouling (Tong et al., 2021); penetrate active sites and pore blocks in adsorption system, thus weakening adsorption capacity (J. Li et al., 2023); and attenuate light reaching the surface

and scavenge reactive radicals during photocatalysis and advanced oxidation, weakening the oxidation efficiency (Ren et al., 2018). This has been formed by the degradation of plant and animal remains, the metabolism of microbes and anthropogenic sources, which bring about NOM. Humic substances, proteins, and polysaccharides form the major part of it. Due to their high molecular weight, complicated spatial conformation and the presence of plenty of reactive functional groups, the polysaccharides tend to have a stronger influence on these processes (Pirozzi et al., 2020; Zeng et al., 2022).

A number of strategies has been suggested in order to reduce the effects of natural polysaccharides in water treatment. Pretreatment, which may be pre-coagulation, pre-oxidation or adsorptionmembrane hybrid is frequently used in membrane systems seeking to decrease the concentration of polysaccharide nearer to the surface of the membrane (Xia et al., 2021). Nevertheless, in photocatalytic systems architectures of catalysts are shaped in a way that facilitates electron-hole separation, and other non-radical oxidation mechanisms are added to reduce radical-scavenging forces (Wang et al., 2022). In adsorption processes competitive interactions are normally reduced by increasing adsorbent dosage or adopting multistage adsorption. These measures are capable of reducing the negative impact of polysaccharides to a zero or minimal degree, but this is not its focal goal and instead, it aims at reducing interference and not taking advantage of polysaccharide structural characteristics to be involved in the pollutant elimination (J. L. Li et al., 2023). It is particularly interesting to note that, natural polysaccharides have the ability to trigger aggregation of particles through ionic bridging thus forming stable flocs which strengthen coagulation, sedimentation and cleaning of contaminants (Yang et al., 2025). Moreover, with the contacts of biochar based composite membranes with natural polysaccharides, a layer-like big and dense gel can be formed on the surface of material, which can in turn enhance adsorptive filtration and pollutant separation (D. Zhang et al., 2022). These results indicate that natural polysaccharides are not simple interferents; their unique structures and chemical reactivity, in the right environment, may be involved and facilitate coagulation and adsorption, and this direction provides a new way of contaminants to work together.

Biochar is a pyrolysis product of biomass generated under oxygen-restricted conditions, which has the characteristic features of a rather high specific surface area, elaborated porosity and

various functional groups as found on the surface (Wang & Zhang, 2020). Biochar is easy to prepare compared to powdered activated carbon and can be made using readily accessible feedstocks, and is more economical, besides showing some encouraging results when used in the removal of BPA (Katibi et al., 2021). However, this effect does not always apply in natural polysaccharides waters, as this adsorption behaviour of traditional fiber-based biochars is usually degraded by competitive forces (Yazdani et al., 2019). A biochar that is produced using shell of crayfish has a high concentration of calcium species in the forms, which is capable of interlocking with natural polysaccharides and produce stable coagulation floc, hence, improving the removable effect of pollutants (D. Zhang et al., 2022). Its highly developed pore structure does not only give it an increased available adsorption sites but also facilitates floc formation and stabilization allowing adsorption with coagulation to take place synergistically (Hakizimana et al., 2025; Kozyatnyk & Njenga, 2023). A synergistic process can be used to reduce the polysaccharide competition to the adsorption sites in addition to enhancing the immobilization of contaminants by further encouraging the use of floc sedimentation. Nevertheless, existing knowledge of the floc formation properties and the performance of coagulation method to remove this kind of bacteria-calcium biochar is very scarce, which shows the necessity of additional research on the prospective of the same in treating water.

In this paper, restaurant-generated crayfish shell waste was adopted as feedstock to process a modified biochar (BCFS800) through oxygen-restrained high-temperature pyrolysis combined with ball milling, developing a material with entirely revealed surface calcium-based units, uniform pore structure and increased functional-group activity. Sodium alginate (SA) was chosen as an example of a natural polysaccharide in water to critically test the possibility of constructing floc using BCFS800-SA synergy in water and its efficiency in extraction of BPA. In order to determine the main factors that control the floc formation stability and also to obtain the right operating conditions, preliminary optimization experiments were performed with the concentration of the SA and the slow mixing rate as the main variables. It is based on this that single-factor experiments were conducted again to provide a systematic study on the influence of pH, temperature, and biochar dosage on the behaviour of floc formation and BPA removal performances in single-factor experiments. Moreover, several characterization methods such as SEM, BET, XRD, FTIR, and XPS were used, to explain the morphology of the structure,

calcium-based crystalline phases, and changes in reactions of chemical bonding, elemental valence states, and surface functional groups of BCFS800 prior to and following treatments. This study aims to verify the mechanism by which BCFS800 and natural polysaccharides synergistically form flocs and enable efficient BPA removal, promoting a conceptual shift of natural polysaccharides from "interfering factors" to functional components for floc construction, and providing new technical insights and theoretical support for efficient removal of organic contaminants and regulation of polysaccharide effects in complex water matrices.

2. Materials and Methods

2.1 Reagents and Instruments

Chemicals：Bisphenol A (BPA), humic acid (HA), bovine serum albumin (BSA), sodium alginate (SA), and all other chemicals used in this study were of analytical grade and were purchased from Tianjin Damao Chemical Reagent Co., Ltd. (China). All chemical solutions were prepared using ultrapure water, which was also used for sample rinsing and cleaning.

Instruments：A jar test apparatus (ZR4-6, Zhongrun Water Science and Technology Development Co., Ltd., China), a muffle furnace (STM-20-17, Henan Sante Furnace Industry Technology Co., Ltd., China), a planetary ball mill (MITR-YXQM-2L), a forced-air drying oven (101-1), a thermostatic magnetic stirrer with heating (DF-101S), and a pH meter (PHS-3C) were used in this study.

2.2Preparation of biochar

Crayfish shell waste collected from a catering company in Chongqing, China, was used as the precursor for biochar production. The crayfish shells were washed, dried, crushed, and sieved through a 100-mesh screen. Biochar was prepared using an oxygen-limited, temperature-programmed carbonization process (Wang et al., 2025). Specifically, the ground crayfish shell samples were placed in ceramic crucibles, sealed with aluminum foil, The crucibles were placed in a muffle furnace at room temperature, and the furnace was then heated to 800 °C at a ramp rate of 10 °C min^{-1} under oxygen-limited conditions. The target temperature of 800 °C was maintained for 2 h. After pyrolysis, the samples were allowed to cool naturally to room temperature inside the furnace before collection.

The resulting biochar was consequently washed with ultrapure water, dried at 105 °C, re-sieved using a 100-mesh sieve, and stored under wraps to be used in subsequent experiments

and ball milling. To obtain smaller biochar particles and improve the physical properties of the material, CFS800 was further modified by planetary ball milling without adding any chemical reagents. Specifically, the biochar sample was mixed with agate balls at a mass ratio of 1:100. The mixture was ball-milled at 300 rpm for 12 h under alternating forward and reverse rotation. Each forward or reverse rotation cycle lasted for 10 min, and the instrument was stopped for 5 min between rotation-direction changes to avoid excessive aggregation of biochar particles during milling. The ball-milled crayfish shell biochar was denoted as BCFS800. The untouched biochar obtained by pyrolyzing at temperature of 800 °C was referred to as CFS800.

2.3 Analytical and Characterization Methods

A concentration of BPA was performed using a UV -visible spectrophotometer (UV-1800PC, Aoyi Instrument Co., Ltd., China) at 278 nm (Ugboka et al., 2022). To reduce possible matrix interference from SA, NOM surrogates, dissolved organic components, and residual fine particles, all supernatant samples were filtered through a 0.45 μm PTFE syringe filter before UV–Vis analysis, and corresponding blank systems without BPA were used for background correction. The BPA calibration curve was Y = 0.0139x + 0.0093, where Y represents the absorbance at 278 nm and x represents the BPA concentration (mg/L), with R^2 = 0.9997..The equation was used to determine the removal efficiency of BPA as follows:

$$\eta = \frac{C_0 - C_t}{C_0} \quad (1)$$

where η is the efficiency of BPA ester removal; C_0(mg/L) is the initial concentration of BPA in the solution; and C_t(mg/L) is the concentration of BPA in the solution at time t.

The dynamic changes in sodium alginate concentration were evaluated by measuring the variation in total organic carbon (TOC) concentration using a TOC analyzer (TOC-LCPH). All batch experiments were conducted in triplicate unless otherwise stated. The results are presented as mean ± standard deviation (SD), and the error bars in the figures represent the standard deviations of triplicate measurements.

The surface morphology and elemental distribution of the resulting biochar was examined with the help of a field-emission-scanning electron-microscope (FE-SEM, Zeiss Sigma) with a security energy-dispersive spectroscopy (EDS) detector attached. The sample characteristics of specific surface area and pore structure were determined through a Micromeritics adsorption

analyzer (ASAP 2020) and changes in the particle size of the biochar in various media were measured with the help of a laser particle size analyzer (Bettersize 3000), and the average particle size was expressed in the form of D50 value. A nanoparticle size and zeta potential analyzer (Brookhaven Instruments Corporation, USA) was used to measure the zeta potential and measure the size of nanoparticles of biochar after experimentation at various pH levels. X-ray diffraction (XRD) patterns of the prepared biochar were recorded using an X'Pert PRO system. X-ray photoelectron spectroscopy (XPS, ESCALAB 250Xi, USA) and Fourier transform infrared spectroscopy (FTIR, Thermo FTIR 5700, USA) were employed to analyze changes in surface functional groups of the crayfish shell–derived biochar before and after BPA removal.After the experiments, supernatant samples were collected at a depth of 2.0 cm below the liquid surface in glass beakers, and the residual turbidity was measured using a turbidimeter (WGZ-4000, Shanghai Xinrui Instrument and Meter Co., Ltd., China).

2.4 Experiments

2.4.1 Coagulation–Floc Formation Experiments

To verify the feasibility of floc formation via crosslinking between BCFS800 and natural polysaccharides, and to distinguish this behavior from the interactions of BCFS800 with other types of natural organic matter (NOM), a series of simulated water matrices was prepared. Humic acid (HA), sodium alginate (SA), and bovine serum albumin (BSA) were employed as representative surrogates for humic substances, polysaccharides, and proteins commonly present in natural waters, respectively. According to different component combinations, seven systems were established: HA only (30 mg/L), SA only (30 mg/L), BSA only (30 mg/L), HA + SA (30 mg/L + 30 mg/L), HA + BSA (30 mg/L + 30 mg/L), SA + BSA (30 mg/L + 30 mg/L), and a ternary mixture of HA + SA + BSA (30 mg/L each). NaCl (0.01 mol/L) was introduced in all systems to bring them to the necessary level of ionic strength.Coagulation experiments were done in a six position jar tester (ZR4-6). In summary, 250 mL of each of the simulated water matrices was poured into an acrylic beaker and subjected to near-neutral conditions at room temperature (pH = 7.0 ± 0.5). Included were parallel experiments and blank controls and 0.5 g of biochar was dosed to each system. The mixing program included rapid mixing at 250 rpm/10 min followed by slow mixing at 50 rpm/10 min that were followed by settling of samples to determine the turbidity and size of floc particles of each system. In the single-component systems, quantification of the

samples collected was done using the 0.45 μm membrane and the final concentrations of HA, BSA and SA were determined by UV–Vis spectrophotometry and total organic carbon (TOC) analysis to determine removal efficiency.

2.4.2 Removal Experiments

The level of gelation and the geometric structure of flocs are controlled by SA concentration, hence, changing the floc size, floc stability and pollutant harvesting (Craciun et al., 2019). The mixing rate, on the contrary, influences the floc growth, structural properties through the control of frequency of collision of the particles, and shear conditions. A suitable slow-mixing stage enhances the growth of the floc but with a porous structure is rather riddled with too high intensity of mixing which will result in floc breakage and/or densification (X. R. Zhang et al., 2022). Based on this, the concentration of the SA and the rate of the mixing were selected as orthogonal screening experimental factors that are likely to support the formation of the floc and maximize the removal of BPA, thus, providing the background to the further single-factor testing. The original concentration of BPA in the simulated water was maintained to be 30 mg/L in order to achieve both representativeness and comparability. This concentration level was decided based on the BPA level that was previously widely employed in the literature and enables clear contrasting between the removal performance under various treatment circumstances. All of the experiments were done at close-neutral pH (pH = 7.0 ± 0.5) and room temperature. Simulated water (250 mL) had been pre-mixed at 250 r/min during 30 s before the dosing where 0.5 g of the prepared BCFS800 was dispersed. A six position jar tester was then used to determine coagulation tests. The mixing program involved rapid mixing at a rate of 250 r/min in 10 min, then slow mixing at the specific level in 10 min after which settling took place in 10 min. Measurement of turbidity was done by removing supernatant at the end of the test at 2 cm below the water surface. A 10 mL syringe was used to collect the aliquots and filter it with a 0.45 mu PTFE syringe filter, and BPA was analyzed. The slow-mixing rate was set at five levels (30, 40, 50, 60, and 70 r/min), and the SA concentration was also set at five levels (30, 40, 50, 60, and 70 mg/L). The orthogonal design made it possible to assess the influence of every factor and its possible impact on the others in a systematic way, which maximized the operating conditions and revealed the most significant

parameters. The best balance of SA concentration and slow-mixing rate, which produces the lowest turbidity with maximum BPA removal, was chosen to be used in the further experiments.

Following the establishment of optimal SA concentration and mixing rate, the effects of other operational factors on BPA removal by ball-milled crayfish shell biochar were examined which included (i) pH (3–10) and (ii) temperature (10–40 °C).

Moreover, to further confirm that the gel-floc construction was effective with the BCFS800–SA synergy in BPA removal and elucidate the significance of the SA activity as a part of the crosslinking mechanism, two alternative systems were developed: gel-floc coagulation system with SA (BCFS800 + SA) and adsorption-only system with BCFS800 only (BCFS800). The experiments conducted above were done under the optimum conditions as presented above to provide reproducibility and representativeness to the experiments. To strengthen the comparison and to elucidate dosage-dependent differences between the two systems, BCFS800 dosage (0.5, 1.0, 1.5, 2.0, 2.5, and 3.0 g/L) was further introduced as a variable, and BPA removal efficiency at different dosages was systematically evaluated. To avoid ambiguity in the optimization procedure, the experimental design was organized into three sequential stages. First, an orthogonal experiment was conducted at a fixed BCFS800 dosage of 2.0 g/L to screen the suitable SA concentration and slow-mixing rate. Second, based on the selected SA concentration and mixing condition, single-factor experiments were carried out to evaluate the effects of pH and temperature on BPA removal. Third, the biochar dosage was further varied to compare the BCFS800–SA system with the BCFS800-only system and to determine the final selected operational condition. Therefore, the BPA removal values obtained in different sections represent different experimental purposes: the orthogonal experiment was used for parameter screening, the dosage-comparison experiment was used to verify the synergistic contribution of SA, and the final removal efficiency was reported under the integrated selected condition.

Table 1. Factor levels for the L25 (5^2) orthogonal design

Levels	Parameters A	Parameters B
	SA concentration （A）/mg/L	Mixing rate （B）/rpm/min
1	30	30

2	40	40
3	50	50
4	60	60
5	70	70

3. Results and Discussion

3.1Floc Construction of BCFS800 in NOM Matrices and the Dominant Role of Polysaccharides

To clarify the properties of floc construction of BCFS800 in multi-component NOM matrices and explain the leading role of polysaccharides, sodium alginate (SA), humic acid (HA), and bovine serum albumin (BSA), were used as model compounds that are the representatives of polysaccharides, humic substances, and proteins in natural waters, respectively. Single-component and mixed systems have been put down to carry out a systematic study of floc formation behavior of BCFS800 and the respective researched removability of organic matter.

As Fig. 1 demonstrates, there were noticeable differences between the systems tested in regard to the removal of organic matter and reduction of turbidity. SA portrayed the best performance in the single-component systems. Following reaction the particle size of BCFS800 changed to about 10.51 μm to 172.11 μm (Fig. 1b). The removal rate of the SA reduced significantly, and the removal efficiency was 82.11%. In the meantime, the turbidity decreased to 4.65 NTU, which was equivalent to an 81.40% turbidity removal. The tendency is probably explained due to the crosslinking between SA and BCFS800, which results in the creation of stable gel-like flocs[18]. This has been recorded in previous studies(Yang et al., 2025; Zhang et al., 2024). In contrast, no evident floc formation was observed in the HA system, where the BCFS800 particle size increased only to 13.66 μm (Fig. 1c). The pasteurated color was 15.16NTU giving a turbidity removal of39.36%. In spite of the fact that the removal of HA became up to 89.78, adsorption and ion exchange were the dominating processes instead of flocculation (Wang & Wang, 2019). The BSA system also did not exhibit any observed flocculation (Fig. 1d): the BCFS800 particle size remained relatively consistent (11.54 μm), turbidity, 32.60 NTU, turbidity removal was insignificant, and BSA removal was lower than 28.32%. These findings suggest that BCFS800 cannot come up with good flocs when BSA is used as the single organic component.

The mixed systems showed a strong increase in the size of the BCFS800 particles at all times in the presence of SA, which proved that SA was of primary value in the formation of flocs. In the case of SA + HA system, floc size was 108.15 μm (Fig. 1e), turbidity was 7.43 NTU, and turbidity was removed by 70.28%. The floc size of the SA + BSA system amounted to 88.57 μm (Fig. 1f), turbidity was 11.73 NTU, as well as the turbidity removal was 53.08%. In the ternary SA + HA + BSA system, the floc size changed further to 74.54 μm (Fig. 1h), turbidity was 14.15 NTU and the turbidity removal was 43.40%. These findings are indicative of the inhibition of floc aggregation and stability by the presence of BSA (Yan et al., 2019), possibly through steric repulsion and /or competitive binding which restricts crosslinking of SA with hydroxyl-calcium species (Yang et al., 2022). HA also influenced floc structure, albeit to a lesser extent; it may be partially embedded within the floc matrix and/or contribute to structural integrity through weak interactions such as hydrogen bonding (Thathsarani et al., 2025). By comparison, the HA + BSA system exhibited a turbidity of 21.80 NTU and a turbidity removal of only 12.80%, with no clear signatures of crosslinking-driven floc formation(Fig. 1g). Overall, these findings demonstrate that SA is the key factor governing floc generation in the BCFS800-based synergistic coagulation system. Therefore, the subsequent removal experiments focused on the single-SA system to more clearly elucidate the removal mechanism under BCFS800–SA synergy.

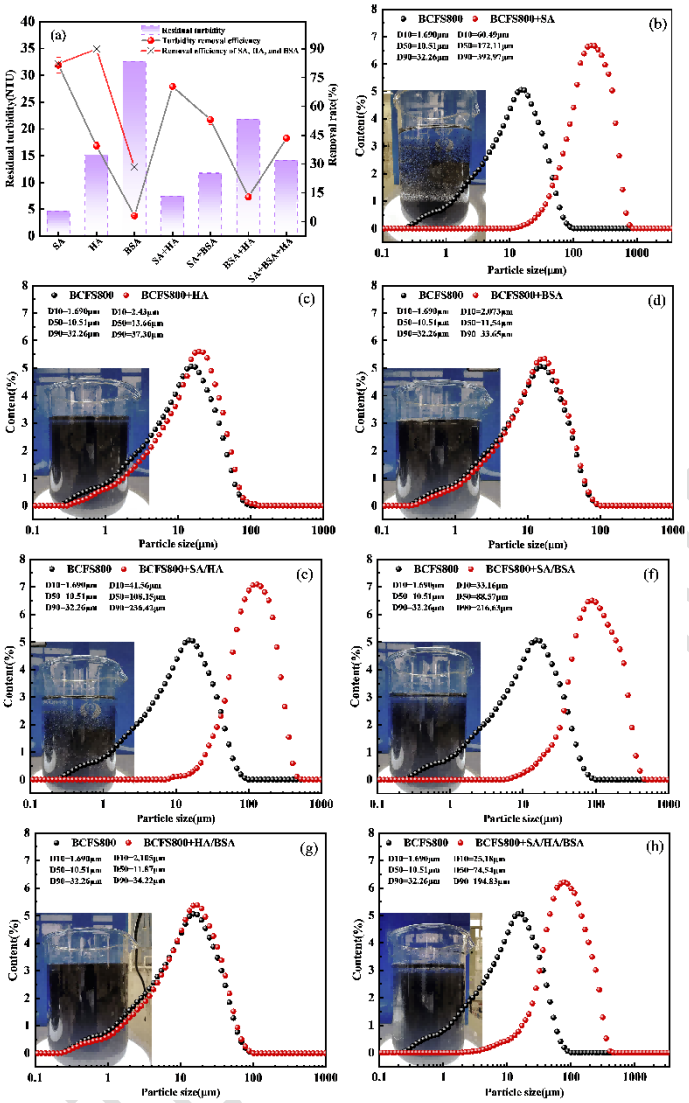

Figure 1. Organic matter and turbidity removal by BCFS800 in different NOM systems (a), and particle size changes of biochar in various simulated systems: (b) SA-only system, (c) HA-only system, (d) BSA-only system, (e) HA/SA mixed system, (f) SA/BSA mixed system, (g) HA/BSA mixed system, and (h) HA/SA/BSA mixed system

3.2 Optimization of Operating Conditions and Pollutant Removal Performance of the BCFS800–Polysaccharide Synergistic System

3.2.1 Synergistic Optimization of SA Concentration and Mixing Rate

Polysaccharide concentration and mixing rate are critical parameters governing floc formation and structural stability, as they determine the extent of crosslinking and the kinetics of particle aggregation, respectively (Huangfu et al., 2013; Sánchez-Martín et al., 2012). To identify

the optimal conditions for generating stable flocs, these two variables were selected as the key factors for optimization. The orthogonal experimental results are summarized in Table 2.BPA removal exhibited a rise–fall trend with increasing SA concentration. According to the range analysis in Table 3, the range of factor A (SA concentration) was 9.77, substantially larger than that of factor B (mixing rate; 4.07), indicating that SA concentration was the primary factor influencing BPA removal. At low SA concentrations (30–40 mg/L), flocs were not fully developed or remained structurally unstable, resulting in relatively poor removal performance. The highest percentage of BPA removal was 66.64 with an SA concentration of 50 mg/L and a mixing rate of 66.64%, which indicates that the crosslinkage between SA molecules and BCFS800 is the most extensive hence the greater the percentage of BPA removal. Another increase of SA to 70 mg/L did trigger a decrease in removal efficiency, however, and some combinations were even worse than 60mg/L. This reduction can be explained by the overabundance of SA which enhances the viscosity of the system and allows the entanglement of the polymer-chains, thus suppressing the pertinent collisions and crosslinking interaction (Dodero et al., 2020).

Other factors that influenced the removal of BPA were mixing rate. Low removal was caused by not enough interparticles collisions at low rate (30 rpm) governing the formation of stable flocs. There was moderate mixing (40-50 rpm) in order to ensure effective contact between the particles but has retained a porous floc structure, hence increasing removal. As the rate was raised to 70 rpm high shear was likely to cause floc break and/or densification, and the removal performance decreased.

Regarding the turbidity reduction, the overall direction was generally similar to that of BPA removal, and this implies that there was a certain level of correlation between the two reactions. The range analysis indicated that factor A (SA concentration) had a range of 10.69 which was slightly higher than factor B (mixing rate; 8.35), indicating that the effect of the SA concentration in turbidity removal was somewhat stronger than the effect of the mixing rate. A proper concentration of SA favoured the growth of the floc and consequently increased the turbidity removal whereas low or excessive concentration of the SA suppressed the growth of the floc and decreased the turbidity removal. Equally, too low mixing rate resulted in fewer contacts between the particles whereas too high resulted in floc breakage, neither of which was desirable in the context of turbidity reduction. The turbidity removal of 91.00% was obtained at a mixing rate of

60 rpm and an SA concentration of 50 mg/L. Consequently, 50mg/L SA and 60rpm were determined to be the standard conditions of later experiments to provide strong floc formation, and the floc performance of the pollutant removal.

Table 2. Results of the orthogonal experiments

Run No.	A	B	Residual BPA concentration (mg/L)	BPA removal efficiency(%)	Turbidity removal efficiency(%)
1	1	1	11.13	49.07	72.51
2	1	2	9.76	52.50	79.15
3	1	3	9.55	55.50	82.96
4	1	4	9.33	55.93	77.27
5	1	5	9.62	56.36	70.91
6	2	1	10.91	55.50	80.08
7	2	2	8.68	59.36	83.10
8	2	3	8.18	61.50	85.75
9	2	4	8.04	62.79	83.30
10	2	5	7.53	63.43	78.66

Table 2(continued).Results of the orthogonal experiments

Run No.	A	B	Residual BPA concentration (mg/L)	BPA removal efficiency(%)	Turbidity removal efficiency(%)
11	3	1	9.26	60.43	84.15
12	3	2	8.90	61.50	86.79
13	3	3	7.96	64.29	89.76
14	3	4	7.03	66.64	91.00
15	3	5	8.11	65.36	84.52
16	4	1	8.97	61.29	84.86
17	4	2	8.54	62.57	85.63
18	4	3	9.04	61.07	88.77

19	4	4	8.83	61.71	88.40
20	4	5	9.33	60.21	82.86
21	5	1	10.34	57.21	82.76
22	5	2	11.06	55.07	84.71
23	5	3	10.63	56.36	88.30
24	5	4	10.48	56.79	84.91
25	5	5	12.06	52.07	76.85

342

343 **Table 3.** Range analysis of the response indicators (BPA removal efficiency and turbidity removal
344 efficiency).

Range analysis	A(BPA)	B(BPA)	A(Turbidity)	B(Turbidity)
K_1	269.36	283.50	382.80	404.36
K_2	302.58	291.00	410.89	419.38
K_3	318.22	298.72	436.22	435.54
K_4	306.85	303.86	430.52	424.88
K_5	277.5	297.43	417.54	393.804
k_1	53.9	56.70	76.56	80.87

345

346 **Table 3**(continued)**.** Range analysis of the response indicators (BPA removal efficiency and
347 turbidity removal efficiency).

Range analysis	A(BPA)	B(BPA)	A(Turbidity)	B(Turbidity)
k_2	60.52	58.20	82.18	83.88
k_3	63.644	59.74	87.25	87.11
k_4	61.37	60.77	86.10	84.98
k_5	55.50	59.49	83.51	78.76
R	9.77	4.07	10.69	8.35

348 3.2.2 Effect of pH

349 The pH of the solution is an important environmental factor that controls the coagulation and
350 adsorption process because it not only determines the speciation of contaminants but also controls

the properties of charge of the functional groups in the surface and formation and stability of flocs (Wang et al., 2016). Fig. 2a shows the performance of the removal under various pH conditions. The highest BPA removal was observed at pH 3. 0 and the maximum efficiency was 70.24%. In acidic conditions (pH 3 to 6) approximately 69% of BPA was removed and 93–95% of the turbidity reduced. With a rise in pH to 8–10, the removal of BPA slowly reduced and finally changed to less than 40% at pH 10; the turbidity removal also reduced, while initially being 91.32%, it dropped to 45.6%.

The system had very high removal performance at low pH (pH 3–7). In this case, the crosslinking of hydroxyl-calcium species on the BCFS800 surface with the SA molecules is possible. When calcium carbonate is partially dissolved in weak acidic media, it yields Ca^{2+} that enhances ionic bridging and the subsequent creation of a stable three-dimensional gel structure (Moreira et al., 2014). Measures of zeta potential revealed that the negative charge on the surface became less negative in the declining pH, consequently, the zeta potential was found to be -0.78 mV at pH 3 that is quite low and, therefore, exhibited minimal electrostatic repulsion. This aids in aggregating particles into small flocs hence significantly increasing the cleaning up of BPA and suspended particulates (Hu et al., 2020). Moreover, BPA mainly exists in its neutral molecular form. Under this pH range, aromatic carbon domains on BCFS800 may act as π-electron-rich sites, facilitating π–π stacking interactions with the aromatic rings of BPA and thereby enhancing BPA retention (Jiang & Hu, 2024).

Once the pH became an alkaline system stability became significantly worse. Zeta potential absolute value rose as the pH rose and maximized it was at pH 10 -25.78 mV, which was more surface-negative and high electrostatic repulsion. This led to increase of the floc structures to be looser and susceptible to fragmentation (Hu et al., 2020). In the meantime, BPA is gradually deprotonating: it starts to change to BPA^{-} at pH ≈ 9.62 and BPA^{2-} predominates at pH > 10.2. Due to the negatively charged surface of the BCFS800, repulsion between strong electrostatic forces in alkaline conditions causes simultaneous decreases in coagulation and total removability (de Lima et al., 2021).

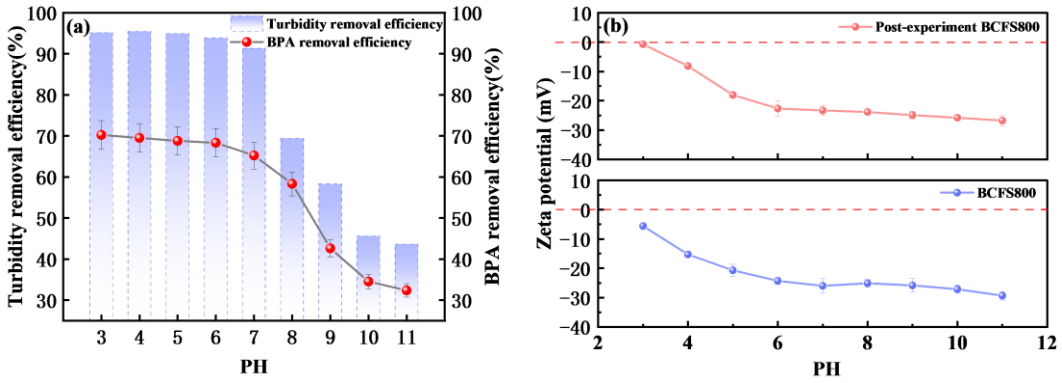

Figure 2. Effect of pH on BPA removal by BCFS800 (a) and the corresponding zeta potential (b).

3.2.3 Effect of Temperature

The temperature is one of the main parameters that influence the velocity and the reaction rates of particles and hence, it also has a significant role in coagulation-based removal. Temperature differences can also affect flocculation and stability of the flocs and the pollutant adsorption processes on the functional groups of biochar (Dlamini et al., 2020). Fig. 3 indicates the removal efficiencies of BPA and turbidity in various temperatures. The BPA removal percentage of 58.57% to 68.81% and turbidity removal of 77.56% to 94.12% indicated that higher temperature facilitated the floc-dominated synergistic removal process, as it increased with the temperature, ranging between 10°C to 40°C, although it slowed at 40 °C. Higher temperature increases the ability of a Brownian motion, resulting in increased frequency of a collision, and adhesion, hence in order to create flocks and to keep the flocs stable more effectively, a more dramatic enhancement in turbidity is observed (Yu et al., 2012). In addition, higher temperature can accelerate the adsorption kinetics of BPA onto biochar surface functional groups, contributing to the observed increase in BPA removal (Carnimeo et al., 2023). The highest removal efficiencies for BPA (68.81%) and turbidity (94.12%) were achieved at 40 °C. Nevertheless, since 40 °C exceeds typical temperatures of natural waters and removal performance was already essentially stable within 25–30 °C, room temperature (25 °C) was selected as the standard condition for subsequent experiments to balance treatment efficiency with environmental representativeness.

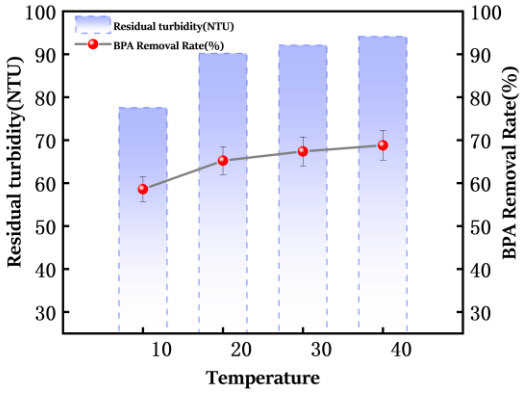

Figure 3. Effect of temperature on BPA removal by BCFS800.

3.3 Verification of the Synergistic Effect of BCFS800 and SA on Removal Performance

Building on the orthogonal screening results, 50 mg/L SA and 60 rpm slow mixing were selected as the basic floc-construction conditions for the following experiments. To further clarify the contribution of SA-induced floc formation to BPA removal, comparative experiments were conducted between the BCFS800–SA system and the BCFS800-only system. It should be noted that this section was not designed to re-screen the SA concentration or mixing rate, but to evaluate the effect of BCFS800 dosage and to verify whether the introduction of SA could enhance BPA removal and solid–liquid separation.

For BPA removal (Fig. 4a), the BCFS800–SA system consistently exhibited higher efficiency than the BCFS800-only system over the whole dosage range. In the BCFS800–SA system, BPA removal increased with increasing biochar dosage, from 48.92% at 0.5 g/L to 71.67% at 2.0 g/L, after which the increase became less pronounced. In contrast, BPA removal in the BCFS800-only system increased from 22.37% to 51.19% with increasing dosage, indicating that the removal in the absence of SA was mainly governed by the number of available adsorption sites on the biochar surface. The value of 71.67% obtained at 2.0 g/L BCFS800 should therefore be understood as the result of the dosage-comparison experiment rather than the final optimized removal efficiency. The occurrence of the SA showed that the presence of the system greatly improved its removal capacity. Such an improvement can probably be explained by the crosslinked floc architecture between the SA molecules and the BCFS800 surface at the aqueous worlds, which allows netting/ sieving capture and synergistic adsorption of BPA and leads to better removal overall(D. Zhang et al., 2022). The stabilization of removal efficiency at dosages of

2.0–3.0 g/L may be related to electrostatic repulsion among negatively charged flocs (Xia et al., 2022). By comparison, the BCFS800-only system mainly relies on surface adsorption, and the increase in available adsorption sites is directly associated with the effective surface area; therefore, removal continued to increase with dosage. At the same dosage, BPA removal in the BCFS800 + SA system was consistently higher than that in the BCFS800-only system, confirming that SA participates in the removal process and contributes to improved performance.

More pronounced differences were observed for turbidity reduction (Fig. 4b). In the BCFS800 + SA system, turbidity removal reached a maximum of 95.70% at 2.0 g/L and then slightly decreased to 84.35% as dosage further increased. This decline may be attributable to residual suspended biochar particles at higher dosages and/or partial disturbance of the established floc structure, and it may also be associated with enhanced interparticle repulsion resulting from changes in floc surface charge (Xia et al., 2022). In contrast, little floc formation occurred in the BCFS800-only system, and turbidity removal remained close to zero throughout the tested dosage range. This observation was consistent with the visual settling behavior during the jar tests: in the absence of SA, BCFS800 particles remained relatively dispersed after mixing and did not form large, rapidly settling flocs.

Compared with previous reports, conventional biochars often show decreased removal performance in the presence of natural polysaccharides. For example, Li et al. (J. Li et al., 2023) reported that polysaccharide fractions in dissolved NOM (with SA as a representative) can compete with target pollutants for adsorption sites on biochar surfaces or form a coating layer, thereby reducing adsorption and removal efficiency. In the present study, however, at a comparable initial BPA concentration (30 mg/L), the removal efficiency of BCFS800 increased by approximately 25–30% in the presence of SA. Instead of presenting a competitive mechanism, SA encouraged the elimination of pollutants, meaning that this type of system successfully surmounted competitive adsorption by natural polysaccharides and a functional change between the competition (interference) and cooperation (synergy). Although the comparison between the BCFS800-only and BCFS800–SA systems provides useful evidence for the enhanced role of SA-induced floc formation, it should be noted that this comparison cannot completely disentangle the individual contributions of adsorption, flocculation, and settling. The BCFS800-only system was used to represent the adsorption-dominated baseline, whereas the enhanced BPA removal and

turbidity reduction in the BCFS800–SA system indicate the involvement of flocculation-assisted removal and improved solid–liquid separation. However, because adsorption, particle aggregation, floc capture, and settling occurred simultaneously in the BCFS800–SA system, their individual contributions could not be quantitatively separated in the present study. Therefore, the enhanced removal performance is interpreted as the result of adsorption-coupled flocculation rather than as evidence for a single independent pathway.

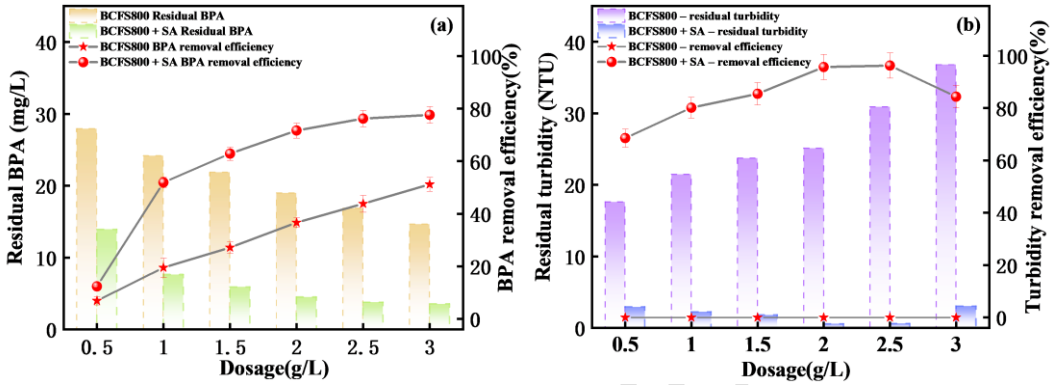

Figure 4. Comparison of BPA removal efficiency (a) and turbidity removal efficiency (b) between systems with and without SA at different biochar dosages.

3.4 Characterization Analysis

To further explain the underlying structural and chemical principle of the significantly improved removal efficiency of the BCFS800–SA synergizing system, the material was analytically described by the pore structure, surface morphology, crystalline phase composition, and elemental chemical states.

3.4.1 Specific Surface Area and Pore Structure Analysis

In order to examine the role of ball-milling modification on the structural properties of the Ca-rich biochar, we measured the N 2 adsorption desorption isotherms of pre-mixed unmilled sample (CFS800) and ball-milled sample (BCFS800) (Fig. 5 and Table 4). To elucidate the regulation of pore structure and specific surface area by ball milling, CFS800 was employed as a reference that can offer structural explanation to the following discussion of the removal mechanisms. Table 4 has summarized and detailed at Fig. 5 that pore architecture of the biochar was significantly improved with ball milling. The surface area of BCFS800 at a specific point (36.15) was changed to 46.42 m^2/g; the volume of the micropore was changed to 0.0036 and then 0.0053 cm^3/g, which showed that ball milling enhanced the formation of micropores and the

number of active sites was exposed. This increase may intensify the adsorption in addition to offering enhanced interfacial bonding sites of SA binding (Wang et al., 2024; H. B. Zhang et al., 2022). Meanwhile, ball milling reduced the total pore volume from 0.1148 to 0.0701 cm^3/g and decreased the average pore diameter from 12.70 to 6.04 nm, suggesting that some macropores and mesopores were sheared and fragmented into smaller pores, resulting in a refined and more uniform pore-size distribution. Such structural evolution produced a denser pore network with improved connectivity, which is favorable for the diffusion and enrichment of pollutant molecules within the carbon matrix (Wu et al., 2022). As shown in Fig. 5, CFS800 exhibited a relatively broad pore-size distribution, whereas BCFS800 featured pores mainly concentrated in the 1–10 nm range, with a more uniform distribution and a more continuous pore network. Taken together with the quantitative data in Table 4, these results demonstrate that ball milling alters the physical structure of the material primarily through "pore refinement–increased accessible surface area."

Table 4 BET analysis results of biochar before and after ball milling

Biochar	Surface area(m^2/g)	Micropore surface area(cm^2/g)	Average pore volume(cm^3/g)	Micropore volume(cm^3/g)	Average pore diameter(nm)
CFS800	36.1479	8.3985	0.107912	0.003613	14.3095
BCFS800	46.4219	12.4468	0.060415	0.005262	6.5846

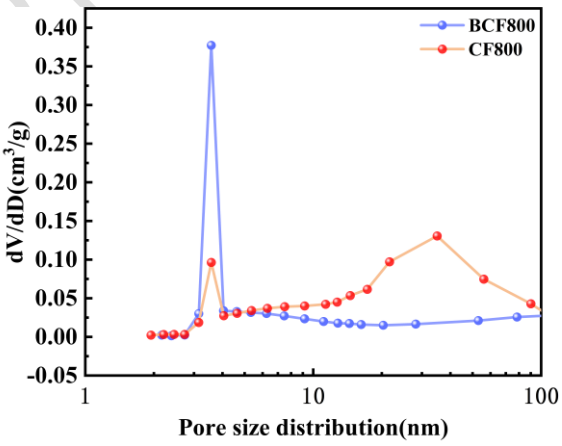

Figure 5. Pore size distribution of CFS800 and BCFS800.

3.4.2 SEM and EDS Mapping

To directly visualize the microstructural features of flocs formed by BCFS800 in the SA system and their elemental distribution, the surface morphology and elemental composition of BCFS800 were analyzed before and after reaction, with CFS800 included as a reference to further elucidate how ball milling activates the biochar structure and enhances interfacial reactivity.

As shown in Fig. 6a, pristine CFS800 exhibited a typical porous network morphology composed of interwoven filamentous carbonaceous components, forming abundant irregular and interconnected pores. This structure likely originates from the release of gases and volatile small molecules during pyrolysis, which promotes the development of a relatively intact pore system on the carbon surface (Jiang et al., 2025). In addition, CFS800 consisted of relatively large, loosely packed particles with locally rough and uneven surfaces, which may be associated with closed pores and/or insufficiently exposed active sites. Conversely, the morphology of the surface of BCFS800 altered significantly following ball milling (Fig. 6c). Ball milling both fractured and further refined the bulk carbon material into much finer nanoscale particles that were packed more densely, as well as effectively removed the amorphous coating of carbon on the pristine biochar to reveal a more regular and honeycomb-like structure lacking a microstructure (Li et al., 2024).

Subsequent analysis of BCFS800 following reaction (Fig. 6e) was found to transform into a highly porous three dimensional network comprising of many particles on the surface. This aspect shows that there was strong interfacial reformation of BCFS800 in the SA system with particles intertwining and stacking up to create a stable floc skeleton. It is worth noting that, even after the formation of flocs, the pores and their surface roughness were still visible in the network implying that some of the original porous properties still remained after the formation of flocs.

These morphological findings were also corroborated by the EDS results (Fig. 6b, d and f). Ball-milled BCFS800 had an increase in surface oxygen content in comparison with CFS800, as 19.24% was replaced with 28.06% suggesting that ball milling contributed to the exposure of oxygen-containing functional groups (Quan et al., 2025). The Ca content fell slightly (38.77% to 36.38%) but at the same time the impurity elements (Na, Mg, K, and S) were reduced, which together with the increase in P we propose that the outer layer was broken off the original particles and made internal Ca-based phases (e.g., $CaCO_3$, $Ca(OH)_2$, and hydroxyapatite) more easily accessible on the face of the material. After reaction, the Ca signal in BCFS800 weakened further, which may be attributed to the participation of Ca-based species at the interface during floc

formation and/or coverage by the newly formed floc matrix, thereby reducing the detectable signal. Meanwhile, the further increase in C and O contents indicates an increased relative proportion of organic components on the post-reaction surface, reflecting pronounced enrichment and coverage of organic matter on the material.

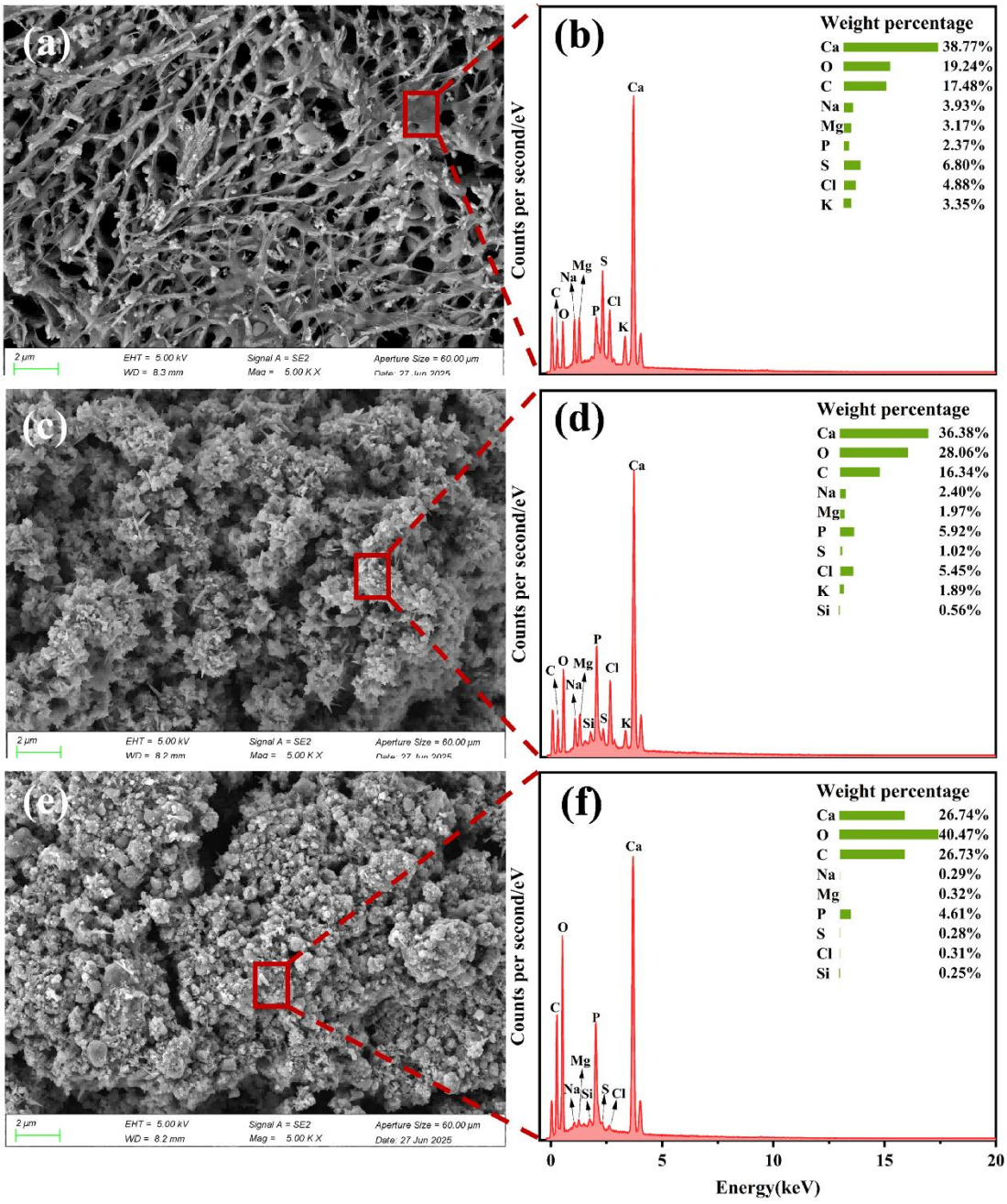

Figure 6. Surface morphology and elemental composition of biochar before and after reaction: (a) and (b) CFS800; (c) and (d) BCFS800; (e) and (f) post-reaction BCSF800.

3.4.3 XRD

To clarify the crystalline-phase composition of BCFS800 during BPA removal in the SA system and its evolution before and after reaction, XRD analysis was performed for BCFS800 samples collected prior to and after treatment, as shown in Fig. 7. The major crystalline phases in BCFS800 were identified as $CaCO_3$ and hydroxyapatite ($Ca_{10}(PO_4)_6(OH)_2$), and the (001) reflection of $Ca(OH)_2$ was also detected (Zhang et al., 2021). These phases are attributable to the decomposition–transformation of $CaCO_3$ during high-temperature calcination at 800 °C: partial $CaCO_3$ decomposes to form $Ca(OH)_2$ and $Ca_{10}(PO_4)_6(OH)_2$. Accordingly, compared with biochar produced at lower calcination temperatures, BCFS800 exhibited weakened $CaCO_3$ peak intensity accompanied by pronounced $Ca(OH)_2$ and $Ca_{10}(PO_4)_6(OH)_2$ peaks (Ai et al., 2017; Oladipo & Ifebajo, 2018).After reaction, the $CaCO_3$ peak at $2\theta = 29.3°$ further decreased in intensity, and the $Ca(OH)_2$ (001) peak at $2\theta = 18.1°$, together with its bulk reflection at $2\theta = 34.1°$, disappeared completely. The disappearance of $Ca(OH)_2$ suggests that it was released from the surface during the reaction, participating in the removal process in dissolved and/or colloidal forms, and ultimately existing as complexes that did not yield detectable crystalline diffraction. The attenuation of $CaCO_3$ peaks may be attributed to the involvement of surface-activated Ca sites in interfacial reactions, which can perturb the near-surface lattice, as well as to coverage of crystal surfaces by the newly formed floc matrix during treatment; both effects would reduce the effective diffracting volume in XRD measurements (Sánchez et al., 2018; J. Zhang et al., 2022). In contrast, hydroxyapatite ($Ca_{10}(PO_4)_6(OH)_2$), owing to its high bond energy and low solubility, exhibited only minor changes after reaction. Although it can participate in crosslinking with SA, this process does not disrupt its lattice structure; consequently, its XRD peaks decreased only slightly.

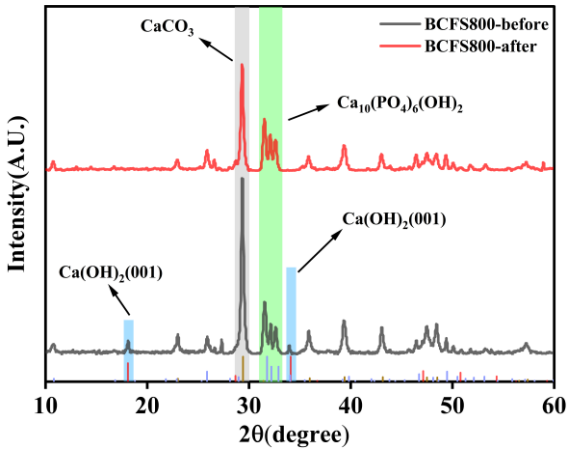

Figure 7. XRD patterns of BCFS800 before and after BPA removal.

553 3.4.4 FTIR

554 To elucidate the evolution of surface functional groups of BCFS800 during BPA removal in
555 the SA system, FTIR spectra of BCFS800 before and after reaction were collected, as shown in
556 Fig. 8. The FTIR spectrum of pristine BCFS800 indicates the presence of abundant surface
557 functionalities. The band at 874 cm^{-1} can be assigned to the bending vibration of aromatic C–H
558 (Yuan et al., 2024). The peak at 1040 cm^{-1} corresponds to the stretching vibration of
559 hydroxyl-associated C–O bonds (Mohd Faizal et al., 2024), while the band at 1430 cm^{-1} is mainly
560 attributed to the stretching vibration of C=O bonds in carbonate structures (Yuan et al., 2024). In
561 addition, the absorption at 1629 cm^{-1} is ascribed to C=C stretching (Shi et al., 2022), and the band
562 at 1792 cm^{-1} is related to the C=O stretching vibration of carboxyl groups (–COOH) (Yao et al.,
563 2024). The peak at 2918 cm^{-1} reflects the stretching vibration of aliphatic C–H (Shi et al., 2022),
564 whereas the broad band spanning 3200–3700 cm^{-1} is attributed to –OH stretching vibrations (Yan
565 et al., 2022).After BPA removal, the aromatic C–H bending band at 874 cm^{-1} decreased markedly,
566 suggesting that aromatic domains on the biochar surface may have strongly adsorbed and stacked
567 with the phenyl rings of BPA through π–π conjugation, thereby restricting the vibrational freedom
568 of C–H bonds (Ahmed et al., 2018). A new band appeared near 1240 cm^{-1}, which is consistent
569 with the C–O stretching vibration of phenolic hydroxyl groups in BPA (Zbair et al., 2020).
570 Meanwhile, the competencies of C=O- and C–O-related bands were reduced considerably,
571 suggesting that the functional groups containing oxygen on biochar were involved in the BPA
572 removal process (Chen et al., 2022). The weakening of the aliphatic C–H band at 2918 cm^{-1} may
573 be associated with hydrogen-bond formation between C–H-containing moieties on the biochar and
574 BPA molecules (Zbair et al., 2020). It is also notable that the O–H vibration peak at 3692 cm^{-1}
575 vanished altogether; this point could also be explained by the fact that it might be due to the
576 activity of the surface $Ca(OH)_2$ to form a gel floc; this assumption is also in line with the results of
577 XRD outcomes.

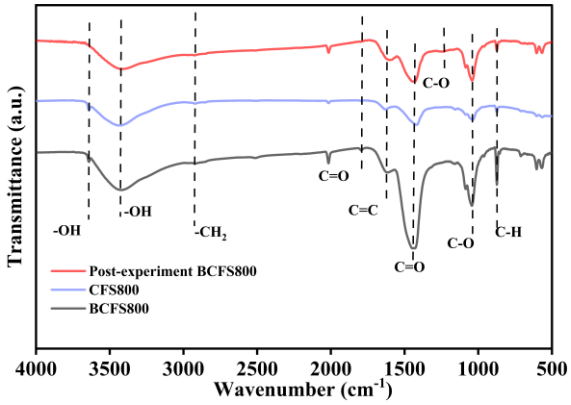

Figure 8. Changes in surface functional groups of biochar before ball milling, after ball milling, and after reaction.

3.4.5 XPS

To elucidate the changes in elemental composition and chemical states of BCFS800 during BPA removal in the SA system, and to verify the interaction mechanism between BCFS800 and SA during the crosslinking process, X-ray photoelectron spectroscopy (XPS) was performed on BCFS800 before and after reaction (Fig. 9). The survey spectra (Fig. 9a) indicate that BCFS800 is mainly composed of Ca, O, and C. Compared with the pristine sample, the post-reaction sample exhibited markedly weakened signals for Ca 2s, Ca 2p, Ca 3s, and Ca 3p, whereas the intensities of the C 1s and O 1s peaks increased substantially; in addition, a Na 1s peak emerged.The high-resolution C 1s spectrum (Fig. 9b) shows that, after reaction, the fraction of C–C decreased from 68.51% to 43.60%, while the contributions of C–O and C=O increased from 9.57% and 21.92% to 35.52% and 23.88%, respectively. The described changes suggest the significant enrichment of oxygen functional groups on the BCFS800 surface that could be the product of the carboxyl and hydroxyl group of SA and the reaction of BPA and functional groups on the BCFS800 surface (Heo et al., 2019; Y. Tian et al., 2024). Consistently, the high-resolution O 1s spectrum (Fig. 9c) shows that the proportion of the C–O component increased from 71.83% to 76.20%, further corroborating the enhancement of oxygenated functionalities inferred from the C 1s analysis.As shown in Fig. 9d, the high-resolution Ca 2p spectrum exhibits a shift of both Ca $2p_{3/2}$ and Ca $2p_{1/2}$ toward lower binding energies after reaction. This shift likely reflects coordination interactions between oxygen-containing functional groups in SA and Ca species

associated with hydroxyl-calcium on the BCFS800 surface, indicating that Ca components played a critical role in interfacial reactions and floc formation (J. Tian et al., 2024).

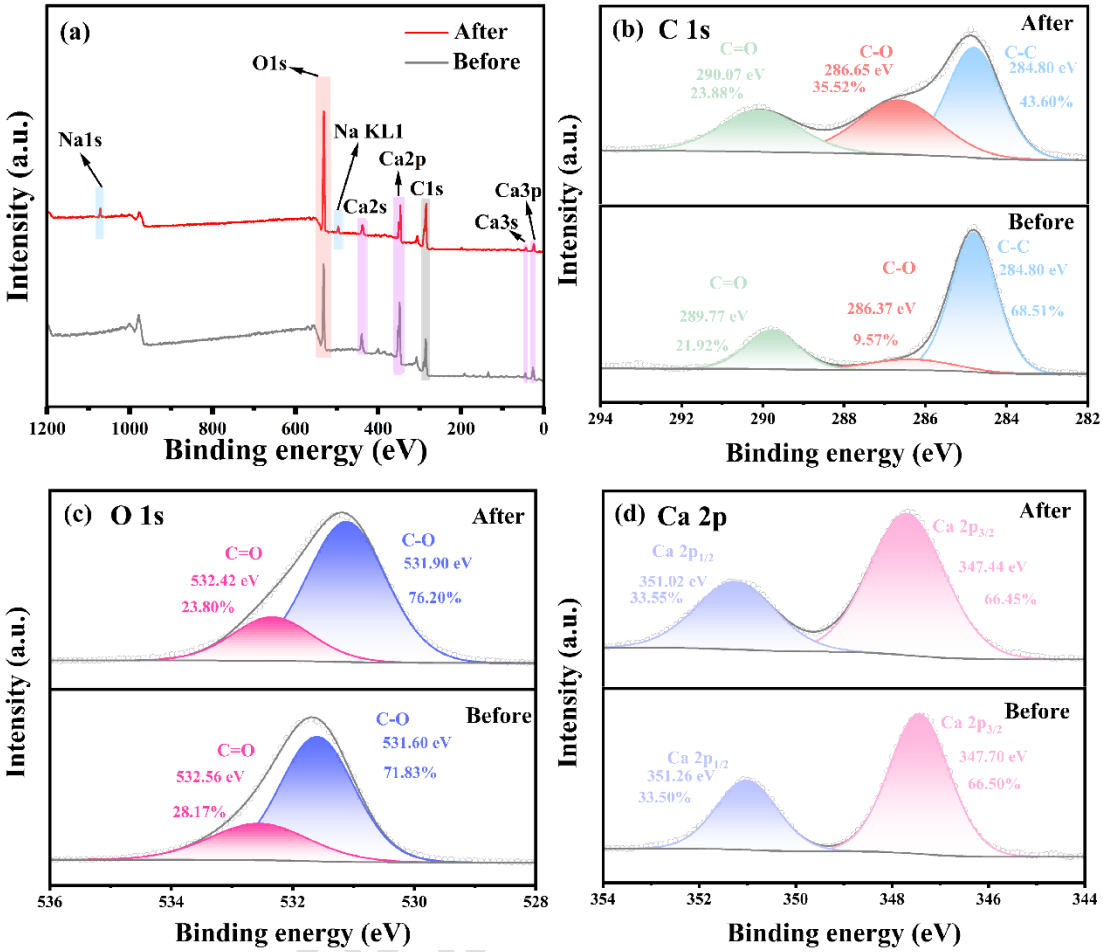

Figure 9. XPS spectra of BCFS800 before and after reaction in the SA system: (a) survey spectra; (b) high-resolution C 1s spectra; (c) high-resolution O 1s spectra; (d) high-resolution Ca 2p spectra.

3.5 Mechanistic Insights into BPA Removal by the BCFS800–SA Synergistic System

Based on the removal performance and characterization results, BPA removal in the BCFS800–SA system can be interpreted as an adsorption-coupled flocculation process. It should be noted that the BET, SEM, XRD, FTIR, and XPS results provide indirect support for the proposed mechanism rather than direct proof of each individual pathway. Therefore, the following discussion is proposed as a plausible interpretation of the observed removal enhancement.

First, BCFS800 provides adsorption sites for BPA enrichment. BET and SEM analyses showed that ball milling increased the specific surface area and exposed more pore structures, which may facilitate BPA diffusion and adsorption. In the BCFS800-only system, BPA removal

616 increased with increasing biochar dosage, indicating that adsorption was the baseline contribution
617 to BPA removal.

618 Second, SA promoted the aggregation of BCFS800 particles and the formation of settleable
619 gel-like flocs. XRD results showed that $Ca(OH)_2$-related peaks decreased or disappeared after
620 reaction, while $CaCO_3$ peaks weakened. Together with SEM observations of a particle-entangled
621 network and XPS evidence of weakened Ca signals and Ca 2p shifts, these results suggest that
622 Ca-based species on BCFS800 may participate in interfacial interactions with SA during floc
623 formation. The resulting floc structure could enhance BPA removal through physical capture and
624 improved solid–liquid separation.

625 Third, FTIR spectral changes suggest that BPA may also be retained through noncovalent
626 interactions. The aromatic structure of BPA may interact with aromatic carbon domains on
627 BCFS800 through π–π interactions, while its phenolic hydroxyl groups may form hydrogen bonds
628 with oxygen-containing functional groups on the biochar or floc surface. These interactions may
629 further contribute to BPA retention within the floc matrix.

630 The comparison between BCFS800-only and BCFS800–SA systems provides a
631 semi-quantitative indication of the synergistic effect. The BCFS800-only system can be regarded
632 as an adsorption-dominated baseline, with BPA removal ranging from 22.37% to 51.19%. In
633 contrast, the BCFS800–SA system achieved higher BPA removal, reaching 71.67% at 2.0 g/L and
634 76.20% under the final selected condition. Thus, the additional removal of approximately 25–35
635 percentage points may be associated with SA-induced floc formation, floc capture, and enhanced
636 settling. However, because adsorption, flocculation, and settling occurred simultaneously, their
637 individual contributions could not be strictly separated in this study.

638 Overall, the enhanced BPA removal in the BCFS800–SA system can be mainly attributed to
639 the coupling of adsorption and flocculation. BCFS800 provides porous adsorption sites, while SA
640 promotes gel-like floc formation through interactions with Ca-based species. BPA may then be
641 removed through adsorption, physical capture, and possible π–π interactions and hydrogen
642 bonding. Therefore, the BCFS800–SA system is more appropriately described as an
643 adsorption-coupled flocculation process rather than a simple adsorption process. Further studies
644 using lower environmentally relevant BPA concentrations, real water matrices, and regeneration
645 tests are still needed to evaluate its practical applicability.

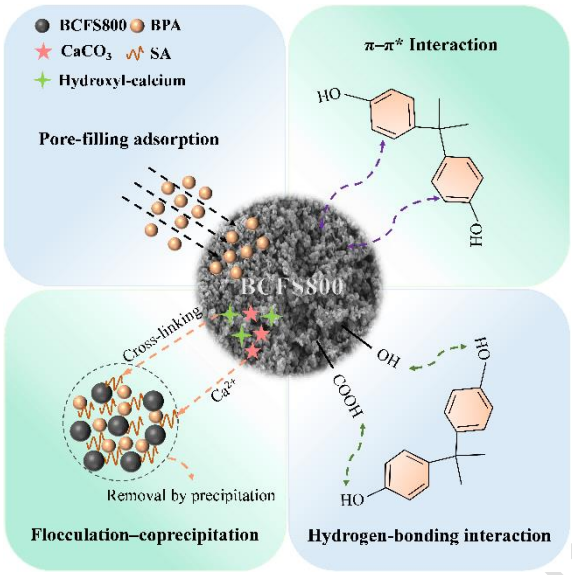

Figure 10. Schematic illustration of the proposed mechanism for BPA removal by the BCFS800–SA system.

3.6 Practical implications and limitations

The BCFS800–SA system provides a potential adsorption-coupled flocculation strategy for BPA removal by combining waste-derived Ca-rich biochar with sodium alginate. Crayfish shell waste is a low-cost and calcium-rich precursor, and this concept may also provide a reference for other calcium-rich biowastes, such as crab shells, shrimp shells, eggshells, or bone-derived materials. Compared with conventional adsorption systems, the BCFS800–SA system may offer the additional advantage of improving both pollutant removal and solid–liquid separation through gel-like floc formation.

However, the present study was mainly conducted in simulated water using an initial BPA concentration of 30 mg/L, which is higher than many environmentally relevant levels. Therefore, the results should be regarded as proof-of-concept and mechanistic evidence rather than direct field-scale validation. Further studies using lower BPA concentrations, real water matrices, and continuous-flow systems are needed to evaluate practical applicability.

In addition, the regeneration, reuse, and disposal of BCFS800–SA flocs were not systematically investigated. The spent flocs should be collected and properly treated before disposal to avoid secondary pollution. Since crayfish shell biochar contains phosphorus-bearing minerals, potential P leaching should also be evaluated in future work. Moreover, SA was used as a representative natural polysaccharide in this study, and other polysaccharides, such as pectin,

xanthan gum, starch, or chitosan, could be further examined to assess the broader applicability of this biochar–polysaccharide synergistic flocculation strategy.

4. Conclusions

(1) The waste shells of crayfish were utilized as the feedstock in this study in order to produce a Ca-based, reactivity-enhanced biochar (BCFS800) through high-temperature pyrolysis and ball milling. Ball milling caused a significant growth in specific surface area of BCFS800 (up to 46.42 m^2/g) and hierarchical pore structure coexisting with micro- and mesopores, which enhanced mass transfer and adsorption of pollutants, compared to the pristine biochar. Meanwhile, ball milling helped access Ca-based crystalline phases, such as $CaCO_3$, $Ca(OH)_2$, and acid carbonate, and significantly lent them a stronger surface reactivity, which gave them many more active sites on which to undergo subsequent crosslinking reactions.

(2) Floc formation experiments revealed that SA had played a leading role as a crosslinking component in multicomponent NOM systems (HA, SA and BSA). SA quickly reacted with Ca-based species on the surface of BCFS800, leading to the formation of tight and solid three-dimensional gel-like flocs, the largest size of the flocs was 172.11 μm and the residual turbidity was lower than 2.13 NTU. The opposite was not true and therefore BSA did not form flocs owing to steric hindrance, but HA was predominantly eliminated by adsorption. Notably, this paper puts forward and confirms a workable metamorphosis of natural polysaccharides; that is, being viewed as factors of interference, to acting as efficient crosslinking carriers; hence offering a mechanistic foundation of follow up experiments of removal.

(3) The BCFS800–SA synergistic system showed improved BPA removal and solid–liquid separation performance under the selected experimental conditions. Based on the optimization results, the selected conditions were BCFS800 dosage of 2.5 g/L, SA concentration of 50 mg/L, initial pH 6, room temperature, and slow-mixing rate of 60 rpm. Under these conditions, the BPA removal efficiency reached 76.20%, and the effluent turbidity remained below 1.0 NTU. The comparison with the BCFS800-only system suggested that SA addition promoted floc formation and improved the overall removal performance. However, because the initial BPA concentration used in this study was 30 mg/L, which is higher than many environmentally relevant concentrations, these results should be interpreted mainly as proof-of-concept and mechanistic evidence rather than direct field-scale treatment performance.

(4) Mechanistic studies found that BPA deposition through gel-like flocs that developed due to the interaction between BCFS800 and SA was fueled by a series of synergistic mechanisms. The porous structure of BCFS800 enabled physical adsorption and enrichment of BPA; Ca-based surface species crosslinked with SA to construct a three-dimensional gel network that encapsulated, adsorbed, and immobilized the pollutant; moreover, reactive groups on the biochar and floc surfaces further interacted with BPA through noncovalent interactions such as hydrogen bonding and π–π stacking, thereby strengthening BPA capture and stabilization.

Acknowledgments

The authors would like to thank the anonymous referees and editors for their careful work and constructive suggestions. This research was financially supported by Chongging Municipal Graduate Educationand Teaching Reform Research Project (YJG233091), Chongqing Municipal Graduate JointIraining Base Construction Project (IDLHPYTD2020025).

References

Abu Hasan, H., Muhamad, M. H., Kurniawan, S. B., Buhari, J., & Abuzeyad, O. H. (2023). Managing Bisphenol A Contamination: Advances in Removal Technologies and Future Prospects. *WATER*, *15*(20), Article 3573.

Ahmed, M. B., Zhou, J. L., Ngo, H. H., Johir, M. A. H., Sun, L., Asadullah, M., & Belhaj, D. (2018). Sorption of hydrophobic organic contaminants on functionalized biochar: Protagonist role of π-π electron-donor-acceptor interactions and hydrogen bonds. *Journal of Hazardous Materials*, *360*, 270-278.

Ai, F., Liu, N., Wang, W., Wang, A., Wang, F., Zhang, H., & Huang, Y. (2017). Heteroatoms-Doped Porous Carbon Derived from Tuna Bone for High Performance Li-S Batteries. *Electrochimica Acta*, *258*, 80-89.

Carnimeo, C., Colatorti, N., D'Orazio, V., Trotti, P., & Loffredo, E. (2023). Potential of Biochar from Wood Gasification to Retain Endocrine Disrupting Chemicals. *MATERIALS*, *16*(2), Article 569.

Chen, H. B., Gao, Y. R., Li, J. H., Sun, C. H., Sarkar, B., Bhatnagar, A., Bolan, N., Yang, X., Meng, J., Liu, Z. Z., Hou, H., Wong, J. W. C., Hou, D. Y., Chen, W. F., & Wang, H. L. (2022). Insights into simultaneous adsorption and oxidation of antimonite [Sb(III)] by crawfish shell-derived biochar: spectroscopic investigation and theoretical calculations. *BIOCHAR*, *4*(1), Article 37.

Craciun, G., Manaila, E., & Ighigeanu, D. (2019). New Type of Sodium Alginate-g-acrylamide Polyelectrolyte Obtained by Electron Beam Irradiation: Characterization and Study of Flocculation Efficacy and Heavy Metal Removal Capacity. *POLYMERS*, *11*(2), Article 234.

de Lima, H. H. C., Llop, M. E. G., dos Santos Maniezzo, R., Moisés, M. P., Janeiro, V., Arroyo, P. A., Guilherme, M. R., & Rinaldi, A. W. (2021). Enhanced removal of bisphenol A using pine-fruit shell-derived hydrochars: Adsorption mechanisms and reusability. *Journal of Hazardous Materials*, *416*, 126167.

Dlamini, N. G., Basson, A. K., & Pullabhotla, R. (2020). Wastewater Treatment by a Polymeric Bioflocculant and Iron Nanoparticles Synthesized from a Bioflocculant. *POLYMERS*, *12*(7), Article 1618.

Dodero, A., Vicini, S., & Castellano, M. (2020). Depolymerization of sodium alginate in saline solutions via ultrasonic treatments: A rheological characterization. *Food Hydrocolloids*, *109*, 106128.

Hakizimana, J. C., Ye, Y., Zhang, F., Ndagijimana, P., Nkinahamira, F., Dusangumukiza, F., Rong, H., Wang, J., Cui, B., & Guo, D. (2025). Carbon-ferric based coagulants for enhanced removal of turbidity, bisphenol A, and tetracycline from synthetic wastewater. *Journal of Water Process Engineering*, *79*, 109011.

Heo, J., Yoon, Y., Lee, G., Kim, Y., Han, J., & Park, C. M. (2019). Enhanced adsorption of bisphenol A and sulfamethoxazole by a novel magnetic CuZnFe2O4–biochar composite. *Bioresource Technology*, *281*, 179-187.

Hu, Y., Yang, Q. Y., Kou, J., Sun, C. B., & Li, H. L. (2020). Aggregation mechanism of colloidal kaolinite in aqueous solutions with electrolyte and surfactants. *PLOS ONE*, *15*(9), Article e0238350.

Huang, M., Xiong, J., Xiao, X., Jiang, Z., Liang, Y., Cai, Y., Zeng, Y., & Chen, Y. (2024). BiOIO3/Bi12SiO20 core-shell S-type heterojunction for efficient photocatalytic removal of bisphenol A: Performance and mechanism study. *Journal of Environmental Chemical Engineering*, *12*(5), 113455.

Huangfu, X. L., Jiang, J., Ma, J., Liu, Y. Z., & Yang, J. (2013). Aggregation Kinetics of Manganese Dioxide Colloids in Aqueous Solution: Influence of Humic Substances and Biomacromolecules. *ENVIRONMENTAL SCIENCE & TECHNOLOGY*, *47*(18), 10285-10292.

Jiang, H., & Hu, H. (2024). Sustainable synergistic adsorption of tetracycline in water by biochar and microplastics: Exploration of the mechanism of DFT. *Journal of Water Process Engineering*, *66*, 105998.

Jiang, H., Ma, J., Zhang, M., Dai, Y., Wang, Y., Huang, H., Yuan, S., Li, K., Zhou, T., Lv, R., Li, K., & Hu, H. (2025). Calcium carbonate self fixed crayfish shell composite biochar for removing tetracycline from water. *Colloids and Surfaces A: Physicochemical and Engineering Aspects*, *711*, 136371.

Katibi, K. K., Yunos, K. F., Man, H. C., Aris, A. Z., Nor, M. Z. M., & Azis, R. S. (2021). An Insight into a Sustainable Removal of Bisphenol A from Aqueous Solution by Novel Palm Kernel Shell Magnetically Induced Biochar: Synthesis, Characterization, Kinetic, and Thermodynamic Studies. *POLYMERS*, *13*(21), Article 3781.

Kozyatnyk, I., & Njenga, M. (2023). Use of biochar and Moringa oleifera in greywater treatment to remove heavy metals and contaminants of emerging concern. *Bioresource Technology Reports*, *24*, 101615.

Li, J., Deng, W., Liu, Z., Pei, B., Ning, S., Cai, Z., & Liu, R. (2023). Detrimental effect of dissolved natural organic matter on molybdenite flotation. *Minerals Engineering*, *193*, 108006.

Li, J. L., Deng, W., Liu, Z. C., Pei, B., Ning, S., Cai, Z., & Liu, R. Z. (2023). Detrimental effect of dissolved natural organic matter on molybdenite flotation. *Minerals Engineering*, *193*, Article 108006.

Li, L. Q., Xie, Y., Chen, K. Y., Zhou, J., Wang, M., Wang, W. Q., Zhang, Z. F., Lu, F., Du, Y. D., & Feng, Y. H. (2024). Adsorption Characteristics of Ball Milling-Modified Chinese Medicine Residue Biochar Toward Quercetin. *ACS OMEGA*, *9*(10), 11658-11670.

Liu, D., Liu, J. N., Guo, M., Xu, H. Z., Zhang, S. H., Shi, L. L., & Yao, C. (2016). Occurrence, distribution, and risk assessment of alkylphenols, bisphenol A, and tetrabromobisphenol A in

surface water, suspended particulate matter, and sediment in Taihu Lake and its tributaries. *Marine Pollution Bulletin*, *112*(1-2), 142-150.

Mohd Faizal, A. N., Putra, N. R., Abdul Aziz, A. H., Agi, A., & Ahmad Zaini, M. A. (2024). Giant mud crab shell biochar: A promising adsorbent for methyl violet removal in wastewater treatment. *Journal of Cleaner Production*, *447*, 141637.

Moreira, H. R., Munarin, F., Gentilini, R., Visai, L., Granja, P. L., Tanzi, M. C., & Petrini, P. (2014). Injectable pectin hydrogels produced by internal gelation: pH dependence of gelling and rheological properties. *Carbohydrate Polymers*, *103*, 339-347.

Noor, S. H. M., Othman, M. H. D., Khongnakorn, W., Sinsamphanh, O., Abdullah, H., Puteh, M. H., Kurniawan, T. A., Zakria, H. S., El-badawy, T., Ismail, A. F., Rahman, M. A., & Jaafar, J. (2022). Bisphenol A Removal Using Visible Light Driven Cu2O/PVDF Photocatalytic Dual Layer Hollow Fiber Membrane. *MEMBRANES*, *12*(2), Article 208.

Oladipo, A. A., & Ifebajo, A. O. (2018). Highly efficient magnetic chicken bone biochar for removal of tetracycline and fluorescent dye from wastewater: Two-stage adsorber analysis. *Journal of Environmental Management*, *209*, 9-16.

Pirozzi, C., Pontoni, L., Fabbricino, M., Bogush, A., & Campos, L. C. (2020). Effect of organic matter release from natural cork used on bisphenol a removal from aqueous solution. *Journal of Cleaner Production*, *244*, 118675.

Quan, B., Chi, D., Xia, G., Liu, X., Chen, W., & Wu, Q. (2025). Ball-milling tailored corn straw biochar: A dramatic shift from physical to chemical adsorption dominance for enhanced ammonia nitrogen removal in source-separated urine. *Industrial Crops and Products*, *235*, 121751.

Ren, M., Drosos, M., & Frimmel, F. H. (2018). Inhibitory effect of NOM in photocatalysis process: Explanation and resolution. *Chemical Engineering Journal*, *334*, 968-975.

Sánchez-Martín, J., Beltrán-Heredia, J., & Peres, J. A. (2012). IMPROVEMENT OF THE FLOCCULATION PROCESS IN WATER TREATMENT BY USING Moringa oleifera SEEDS EXTRACT. *BRAZILIAN JOURNAL OF CHEMICAL ENGINEERING*, *29*(3), 495-501.

Sánchez, M., Vásquez-Quitral, P., Butto, N., Díaz-Soler, F., Yazdani-Pedram, M., Silva, J. F., & Neira-Carrillo, A. (2018). Effect of Alginate from Chilean Lessonia nigrescens and MWCNTs on CaCO3 Crystallization by Classical and Non-Classical Methods. *CRYSTALS*, *8*(2), Article 69.

Shi, G., He, S., Chen, G., Ruan, C., Ma, Y., Chen, Q., Jin, X., Liu, X., He, C., Du, C., Dai, H., & Yang, X. (2022). Crayfish shell-based micro-mesoporous activated carbon: Insight into preparation and gaseous benzene adsorption mechanism. *Chemical Engineering Journal*, *428*, 131148.

Sujatha, A. R., Krishnan, S., & Suneesh, C. V. (2025). Post-synthetic amination of porous hypercrosslinked polymer for the adsorptive removal of bisphenol-A from water. *RSC Applied Polymers*, *3*(6), 1482-1494.

Thathsarani, N., Najafi, M., Khiadani, M., Azhar, M. R., & Zargar, M. (2025). Integrated Chitosan-based coagulation and microbubble pre-treatment for improved microplastic fibre removal from water. *Science of The Total Environment*, *1009*, 181039.

Tian, J., Bu, P., Gao, S., & Geng, M. (2024). New insights into the influence of ultrafiltration pretreatment on reverse osmosis membrane fouling during urban sewage reclamation:

Interaction between extracellular polymeric substances and inorganic foulants. *Journal of Environmental Chemical Engineering*, *12*(6), 114368.

Tian, Y., Sun, X., Chen, N., Cui, X., Yu, H., Feng, Y., Xing, D., & He, W. (2024). Efficient removal of hexavalent chromium from wastewater using a novel sodium alginate-biochar composite adsorbent. *Journal of Water Process Engineering*, *64*, 105655.

Tian, Z. L., Zhang, L. P., & Ni, C. H. (2019). Preparation and flocculation properties of modified alginate amphiphilic polymeric nano-flocculants. *Environmental Science and Pollution Research*, *26*(31), 32397-32406.

Tong, X., Zhao, X. H., Wu, Y. H., Bai, Y., Ikuno, N., Ishii, K., & Hu, H. Y. (2021). The molecular structures of polysaccharides affect their reverse osmosis membrane fouling behaviors. *JOURNAL OF MEMBRANE SCIENCE*, *625*, Article 118984.

Ugboka, U. G., Ihedioha, J. N., Ekere, N. R., & Okechukwu, F. O. (2022). Human health risk assessment of bisphenol A released from polycarbonate drinking water bottles and carbonated drinks exposed to sunlight in Nigeria. *INTERNATIONAL JOURNAL OF ENVIRONMENTAL ANALYTICAL CHEMISTRY*, *102*(12), 2830-2840.

Wang, B., Ma, Y. Y., Cao, P., Tang, X. D., & Xin, J. L. (2024). Ball Milling and Magnetic Modification Boosted Methylene Blue Removal by Biochar Obtained from Water Hyacinth: Efficiency, Mechanism, and Application. *MOLECULES*, *29*(21), Article 5141.

Wang, J., & Wang, S. (2019). Preparation, modification and environmental application of biochar: A review. *Journal of Cleaner Production*, *227*, 1002-1022.

Wang, J. P., & Zhang, M. (2020). Adsorption Characteristics and Mechanism of Bisphenol A by Magnetic Biochar. *INTERNATIONAL JOURNAL OF ENVIRONMENTAL RESEARCH AND PUBLIC HEALTH*, *17*(3), Article 1075.

Wang, W., Wu, H., Sun, J., Zhai, C., Song, J., Chen, D., Yang, G., Dai, Y., Wang, S., & Kong, F. (2025). Enhanced removal of Cr (VI) in constructed wetland with Fe-Ni-LDH-modified crayfish shell biochar: Performance, removal pathways and synergy mechanisms of substrate-microorganism. *Journal of Hazardous Materials*, *497*, 139724.

Wang, Y. J., Wu, C. D., Duan, Y., & Zhang, Z. L. (2016). Removal of pollutants by enhanced coagulation combined PAC with variable charge soils: flocs' properties and effect of pH. *ENVIRONMENTAL TECHNOLOGY*, *37*(18), 2273-2280.

Wang, Z., Li, Q., Su, R., Lv, G., Wang, Z., Gao, B., & Zhou, W. (2022). Enhanced degradation of bisphenol F in a porphyrin-MOF based visible-light system under high salinity conditions. *Chemical Engineering Journal*, *428*, 132106.

Werkneh, A. A., Gebru, S. B., Redae, G. H., & Tsige, A. G. (2022). Removal of endocrine disrupters from the contaminated environment: public health concerns, treatment strategies and future perspectives - A review. *Heliyon*, *8*(4), e09206.

Wu, J. Q., Wang, T. S., Liu, Y. Y., Tang, W., Geng, S. Y., & Chen, J. W. (2022). Norfloxacin adsorption and subsequent degradation on ball-milling tailored N-doped biochar. *Chemosphere*, *303*, Article 135264.

Xia, S. J., Zhang, X. R., Zhao, Y. C., Tan, F. J., Li, P., & Liu, Y. L. (2021). Effect of Pre-Oxidation on Coagulation/Ceramic Membrane Treatment of Yangtze River Water. *MEMBRANES*, *11*(5), Article 369.

Xia, Y., Li, W. J., He, X. W., Liu, D. N., Sun, Y. C., Chang, J., & Liu, J. (2022). Efficient Removal of Organic Matter from Biotreated Coking Wastewater by Coagulation Combined with Sludge-Based Activated Carbon Adsorption. *WATER*, *14*(15), Article 2446.

Yan, C., Cheng, T., & Shang, J. (2019). Effect of bovine serum albumin on stability and transport of kaolinite colloid. *WATER RESEARCH*, *155*, 204-213.

Yan, L., Dong, F.-X., Li, Y., Guo, P.-R., Kong, L.-J., Chu, W., & Diao, Z.-H. (2022). Synchronous removal of Cr(VI) and phosphates by a novel crayfish shell biochar-Fe composite from aqueous solution: Reactivity and mechanism. *Journal of Environmental Chemical Engineering*, *10*(2), 107396.

Yang, W., Li, B., & Shang, J. (2022). Aggregation kinetics of biochar nanoparticles in aqueous environment: Interplays of anion type and bovine serum albumin. *Science of The Total Environment*, *833*, 155148.

Yang, X., Zhang, D., Xue, Y., Liang, J., Tu, Z., Lv, Y., & Zhang, Z. (2025). Traditional gel nanofiltration membranes doped with ball-milled crayfish shell biochar for high-selectivity dye/salt separation. *Journal of Environmental Chemical Engineering*, *13*(3), 116967.

Yao, X.-W., Chen, X., Chen, M.-L., Feng, N.-J., Tong, L.-Y., Yi, Y.-Q., Qian, W., & Diao, Z.-H. (2024). Removal of pesticide acetamiprid using KOH activated biochar derived from crayfish shell: Behavior and mechanism. *Process Safety and Environmental Protection*, *186*, 808-818.

Yazdani, M. R., Duimovich, N., Tiraferri, A., Laurell, P., Borghei, M., Zimmerman, J. B., & Vahala, R. (2019). Tailored mesoporous biochar sorbents from pinecone biomass for the adsorption of natural organic matter from lake water. *Journal of Molecular Liquids*, *291*, Article 111248.

Yu, R., Yang, Y. L., Zhou, Z. W., Li, X., Liu, C. J., Wang, N., & Liu, Y. W. (2023). Attribution of photocatalysis of fluorescent natural organic matter fractions to the alleviation of ceramic membrane ultrafiltration fouling. *Separation and Purification Technology*, *307*, Article 122603.

Yu, W.-z., Liu, T., Gregory, J., Li, G.-b., Liu, H.-j., & Qu, J.-h. (2012). Aggregation of nano-sized alum–humic primary particles. *Separation and Purification Technology*, *99*, 44-49.

Yuan, Y., Wu, Q., Cao, W., Fang, S., Cao, J., Liu, W., & Luo, J. (2024). Recycling crayfish shell and waste activated sludge as biochar to in-situ enhance antibiotics removal from wastewater: Linking structure properties and reaction kinetics. *Journal of Water Process Engineering*, *63*, 105517.

Zbair, M., Bottlinger, M., Ainassaari, K., Ojala, S., Stein, O., Keiski, R. L., Bensitel, M., & Brahmi, R. (2020). Hydrothermal Carbonization of Argan Nut Shell: Functional Mesoporous Carbon with Excellent Performance in the Adsorption of Bisphenol A and Diuron. *WASTE AND BIOMASS VALORIZATION*, *11*(4), 1565-1584.

Zeng, B., Pan, Z., Shen, L., Zhao, D., Teng, J., Hong, H., & Lin, H. (2022). Effects of polysaccharides' molecular structure on membrane fouling and the related mechanisms. *Science of The Total Environment*, *836*, 155579.

Zhang, D., He, Q., Hu, X., Zhang, K., Chen, C., & Xue, Y. (2021). Enhanced adsorption for the removal of tetracycline hydrochloride (TC) using ball-milled biochar derived from crayfish shell. *Colloids and Surfaces A: Physicochemical and Engineering Aspects*, *615*, 126254.

Zhang, D., Ma, L., Da, Y., Li, W., Chen, M., Hu, K., Meng, X., Chen, Y., & Qin, Y. (2024). Enhanced biofouling resistance of polyvinylidene fluoride ultrafiltration membranes using crayfish shell

biochar with calcium species. *Journal of Environmental Chemical Engineering*, *12*(6), 114825.

Zhang, D., Zhang, K., Chen, K., Xue, Y., Liang, J., & Cai, Y. (2022). Mitigation of organic fouling of ultrafiltration membrane by high-temperature crayfish shell biochar: Performance and mechanisms. *Science of The Total Environment*, *820*, 153183.

Zhang, H. B., Su, L., Cheng, C. P., Cheng, H. Y., Chang, M. C., Liu, F. W., Liu, N., & Oh, K. (2022). A new type of calcium-rich biochars derived from spent mushroom substrates and their efficient adsorption properties for cationic dyes. *FRONTIERS IN BIOENGINEERING AND BIOTECHNOLOGY*, *10*, Article 1007630.

Zhang, J., Cao, Y. P., & Xu, D. X. (2022). Encapsulation of calcium carbonate with a ternary mixture of sodium caseinate/gelatin/xanthan gum to enhance the dispersion stability of solid/oil/water emulsions. *FRONTIERS IN NUTRITION*, *9*, Article 1090827.

Zhang, X. R., Zhu, J. Q., Li, Z. X., Li, J. Y., & Ren, P. F. (2022). Effect of hydrodynamic breakage on floc evolution and turbidity reduction in flocculation and sedimentation processes. *WATER SUPPLY*, *22*(2), 1409-1420.